

Article

Molecular Structure and Electronic Properties of Triolein Molecule under an External Electric Field Related to Streamer Initiation and Propagation

Yachao Wang, Feipeng Wang *, Jian Li *, Zhengyong Huang, Suning Liang and Jinghan Zhou

The State Key Laboratory of Power Transmission Equipment and System Security and New Technology, College of Electrical Engineering, Chongqing University, Chongqing 400044, China; wangyachao@cqu.edu.cn (Y.W.); yaahook@163.com (Z.H.); suningliang@cqu.edu.cn (S.L.); zhoujinghan0511@hotmail.com (J.Z.)

* Correspondence: fpwang@cqu.edu.cn (F.W.); lijian@cqu.edu.cn (J.L.);
Tel.: +86-023-65102434 (F.W.); +86-023-65102437 (J.L.)

Academic Editor: Paul L. Chen

Received: 9 March 2017; Accepted: 6 April 2017; Published: 10 April 2017

Abstract: Natural ester has been widely studied as an alternative dielectric liquid to mineral oil in recent years. Unsaturated triacylglycerol molecules are the main components of natural ester; therefore, in this paper, we investigate the molecular structure and electronic properties of the triolein molecule, an oleic-type triacylglycerol molecule, as a representative component of natural ester oils. The effects of external electric fields at the electric field intensity related to streamer initiation and propagation on the bond lengths, dipole moment, total energy, infrared spectra, and orbital energy of the triolein molecule are investigated using density functional theory (DFT). In addition, the excitation energies, transition wavelengths, and oscillator strengths of the first eight excited states of the triolein molecule under external electric fields are calculated by time-dependent DFT. The results show that the bond lengths, dipole moments, total energy, and infrared spectra change obviously under external electric fields. With increasing external electric field intensity, the energy of the highest occupied molecular orbital increases, and the gap between that and the energy of the lowest unoccupied molecular orbital decreases, which make the molecule susceptible to excitation. The calculations contribute to an understanding of the causes behind the degradation of the insulation properties of natural ester oils.

Keywords: nature ester; streamer; triolein molecule; electric field; density functional theory; excited states

1. Introduction

In recent years, natural ester has been studied widely as an alternative dielectric liquid to mineral oil in transformers and disconnectors [1–9]. Natural esters are biodegradable and environmentally friendly. Natural esters are 97% decomposed after 21 days by the CEC-L-33 test [1,2] and, therefore, present little threat to soil and watercourses when released into the environment. The environmental benefits of natural esters make the use of this material increasingly attractive. In addition, the fire point of natural esters is above 300 °C, which is significantly greater than that of mineral oils (~160 °C) [3]. Therefore, natural ester also offers better fire resistance than mineral oil.

It is well known that dielectric liquids are subject to dielectric breakdown accompanied by the development of streamers. A streamer is a gas/plasma filled channel that initiates and propagates in a region with high electric fields and is, therefore, usually created at metallic protrusions and at sharp edges. A streamer is driven in the process of propagation by a continuous liberation and capture of electrons, accompanying by complex sound and light effects. The molecules comprising the

dielectric act as sources of electrons and the electronic properties of the molecules play an important role in streamer initiation and propagation. Many studies have investigated streamer propagation and breakdown in natural esters under high-voltage conditions [10–17]. Propagation tests have shown that streamers propagate faster and further in natural ester than in mineral oil under an equivalent applied electric field. This low resistance to fast streamers has been shown in breakdown tests with various gap distances that natural esters have a lower breakdown voltage than mineral oil.

Streamers are divided into four modes according to their propagation rate, and modes 1–4 are roughly divided in the respective order of 100 m/s, 1 km/s, 10 km/s, and 100 km/s. Streamers propagate in the first mode at very low applied voltages, and propagate in the second mode at around the breakdown voltage, where the electric field intensity necessary to maintain streamer propagation is about 10^8 V/m [18–20]. If the electric field stress is too weak, streamers may cease propagating before reaching the opposite electrode. When the applied voltage increases beyond the breakdown voltage, the propagation rate of streamers changes abruptly from the second to the third mode and, eventually, to the fourth mode at the so-called acceleration voltage. Under the acceleration voltage, a relatively high concentration of molecules are ionized, and the fast-moving electrons leave the much slower positive ions while running to the positive electrode. The enhanced electric field owing to the increased concentration of space charges can further increase the propagation rate of streamers. The electric field stress in the third and fourth modes must be at least 10^9 V/m [21]. In addition, the molecular structure and electronic properties of molecules are altered under a high electric field stress, and these changes may affect the initiation and propagation of streamers.

In this paper, we investigate the molecular structure and electronic properties of a natural ester molecule under external electric fields ranging from -25.7×10^8 V/m to 25.7×10^8 V/m using density functional theory (DFT) and time dependent density functional theory (TD-DFT). The calculations contribute to an understanding of the causes behind the degradation of the insulation properties of natural ester.

2. Theoretical Method

Triacylglycerol molecules account for greater than 95% of the content of natural esters. Figure 1 presents the structure of the triacylglycerol molecule in which R, R', and R'' represent different fatty acids. Since natural esters include hundreds of saturated and unsaturated triacylglycerol molecule types, a complete evolutionary simulation of their electronic properties is not feasible. However, we note that natural ester oils contain a greater proportion of unsaturated triacylglycerol molecules than saturated triacylglycerol molecules [22]. Therefore, the triolein molecule, which is an oleic-type polar triacylglycerol molecule with a mono C=C bond, is chosen to serve as a representative molecule to investigate the electronic properties of triacylglycerol molecules under external electric fields.

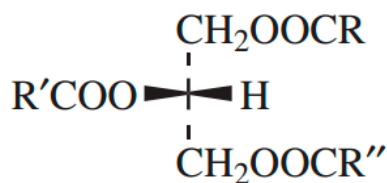


Figure 1. Triacylglycerol molecule.

Figure 2 illustrates the structure of the triolein molecule. The geometry of the triolein molecule was first optimized under no external electric field using DFT with Becke's three-parameter hybrid functional combined with the electron-correlation functional of Lee, Yang, and Parr (B3LYP) prescription [23,24] employing the 6-31G* basis set. A permanent dipole moment of 6.59 Debye was calculated, and the orientation is shown by the blue arrow in Figure 2. External electric fields were applied along the Z axis, respectively, and included electric field intensities of -0.0050 a.u.,

−0.0025 a.u., −0.0010 a.u., −0.0005 a.u., 0.0005 a.u., 0.0010 a.u., 0.0025 a.u., and 0.0050 a.u., where 1 a.u. = 5.14×10^{11} V/m (namely, -25.7×10^8 V/m, -12.9×10^8 V/m, -5.14×10^8 V/m, -2.57×10^8 V/m, 2.57×10^8 V/m, 5.14×10^8 V/m, 12.9×10^8 V/m, and 25.7×10^8 V/m, respectively). The geometry of the triolein molecule was optimized under different external electric fields using the same method discussed above. Nine types of ground state geometries were obtained in total.

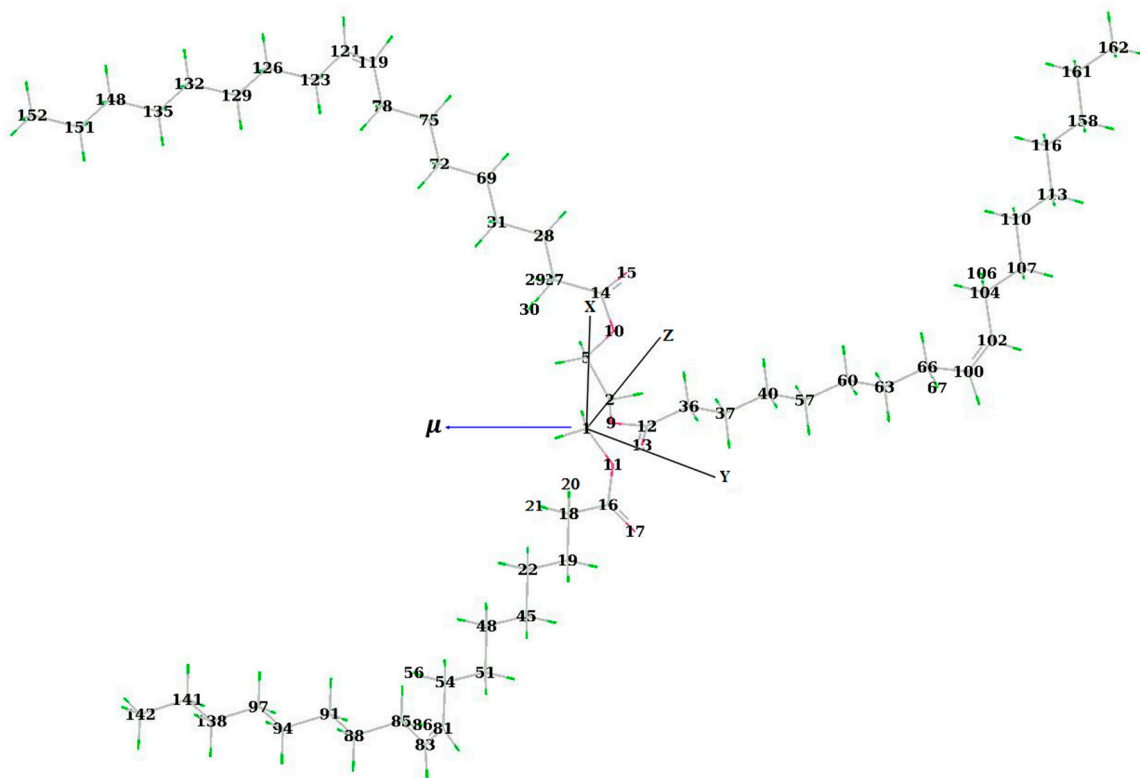


Figure 2. Geometry of the triolein molecule with a Cartesian axis. The blue arrow is the orientation of the permanent dipole moment. C atoms, O atoms, and segmental H atoms are labeled. Gray: C, red: O, green: H.

The Hamiltonian of the molecule system under an external electric field is rewritten as [25]:

$$H = H_0 + H_{\text{int}} \quad (1)$$

where H_0 is the molecule Hamiltonian and H_{int} is the interaction Hamiltonian between the electric field and the molecule, which is approximated as:

$$H_{\text{int}} = -\boldsymbol{\mu} \cdot \boldsymbol{F} \quad (2)$$

where \boldsymbol{F} is the radiation field and $\boldsymbol{\mu}$ is the dipole moment. Time-dependent DFT (TD-DFT) with the B3LYP/6-31G* scheme was employed to investigate the first eight excited states based on the above obtained geometries. The excitation energy is given as:

$$E_{\text{ex}}(\boldsymbol{F}) = E_{\text{ex}}(0) - \Delta\boldsymbol{\mu} \cdot \boldsymbol{F} - \frac{1}{2}\Delta\alpha\boldsymbol{F}^2 \quad (3)$$

where $E_{\text{ex}}(0)$ is the excitation energy without electric field, $\Delta\boldsymbol{\mu}$ is the variation in the dipole moment, and $\Delta\alpha$ is the variation in the polarizability [26,27]. The calculations were conducted using the Gaussian 09 program package [28].

3. Results and Discussion

3.1. Vibrational Frequencies of the Functional Groups of the Triolein Molecule under No External Electric Field

The main functional groups of the triolein molecule are C=O and C=C *cis* double bonds. The vibrational frequencies of these functional groups were investigated. A scale factor of 0.960 was employed with the B3LYP/6-31G* scheme to address the fundamental error raised in an earlier work [29]. The results are listed in Table 1 together with previously published experimental data [30,31]. The vibrational frequencies obtained for C=O stretching were 1775.7 cm⁻¹, 1778.2 cm⁻¹, and 1784.9 cm⁻¹ from C12=O13, C14=O15, and C16=O17, respectively. The vibrational frequencies obtained for C=C *cis* stretching were 1673.4 cm⁻¹, 1673.5 cm⁻¹, and 1673.6 cm⁻¹ from C81=C83, C100=C102, and C119=C121, respectively. The values obtained from DFT are close to those of the experimental results.

Table 1. The vibration frequencies of functional groups.

Method/Scale Factor	Vibration Frequency (cm ⁻¹)	
	C=O Stretching	C=C <i>cis</i> Stretching
B3LYP/6-31G*/0.960 ¹	1775.7, 1778.2, 1784.9	1673.4, 1673.5, 1673.6
Experimental	1746 ² , 1745 ³	1653 ² , 1654 ³

¹ Scale factor data are taken from [29]. ^{2,3} Experimental data are taken from [30,31], respectively.

3.2. Bond Lengths, Total Energy, and Dipole Moment of the Triolein Molecule under Different External Electric Fields

As discussed, changes in structural parameters often contribute to the emergence of new electrical properties. Due to space limitations, only a partial listing of bond lengths for the triolein molecule are presented in Table 2. The results show that the lengths of carbon-oxygen bonds change obviously with increasing electric field intensity. With the application of an external electric field intensity of 25.7×10^8 V/m, we note that the bond length of R(C16-O11) is lengthened 0.0079 Å from 1.3767 Å to 1.3846 Å, and the bond length of R(C14-O10) is shortened 0.0112 Å from 1.3715 Å to 1.3603 Å. Variations in the carbon-carbon bond lengths are relatively slight, particularly the C=C double bonds, although changes in the bonds are quasi-paralleled to the direction of the electric field. We note that the bond length of R(C100=C102) is lengthened by only 0.0002 Å from 1.3391 Å to 1.3393 Å when the external electric field intensity is increased from 0 V/m to 25.7×10^8 V/m.

Table 2. Select bond lengths R of the triolein molecule under different external electric field intensities E.

E (10 ⁸ V/m)	R(C1-C2) (Å)	R(C12-O9) (Å)	R(C14-O10) (Å)	R(C14=O15) (Å)	R(C16-O11) (Å)	R(C16=O17) (Å)	R(C100=C102) (Å)
-25.7	1.5299	1.3877	1.3806	1.2012	1.3715	1.2081	1.3393
-12.85	1.5297	1.3843	1.3759	1.203	1.3715	1.2064	1.3391
-5.14	1.5295	1.382	1.3733	1.2042	1.3754	1.2056	1.3391
-2.57	1.5295	1.3812	1.3724	1.2046	1.3761	1.2053	1.3391
0	1.5295	1.3804	1.3715	1.205	1.3767	1.2051	1.3391
2.57	1.5295	1.3796	1.3706	1.2054	1.3773	1.2049	1.3391
5.14	1.5295	1.3787	1.3698	1.2058	1.3779	1.2047	1.3391
12.85	1.5295	1.376	1.3672	1.2071	1.3798	1.2042	1.3392
25.7	1.529	1.3709	1.3603	1.2101	1.3846	1.2028	1.3393

The dipole moment of the triolein molecule was calculated under different external electric field intensities, and the results are shown in Figure 3. The calculated dipole moment is the resultant of the permanent dipole moment and the dipole moment induced by the external electric field. The orientation of the induced dipole moment is opposite to that of the external electric field. Hence, the dipole moment of the triolein molecule first decreased and then increased with the application of an increasing negative external electric field intensity, and increased continuously with the application

of an increasing positive external electric field up to 15.88 Debye when an external electric field of 25.7×10^8 V/m was applied.

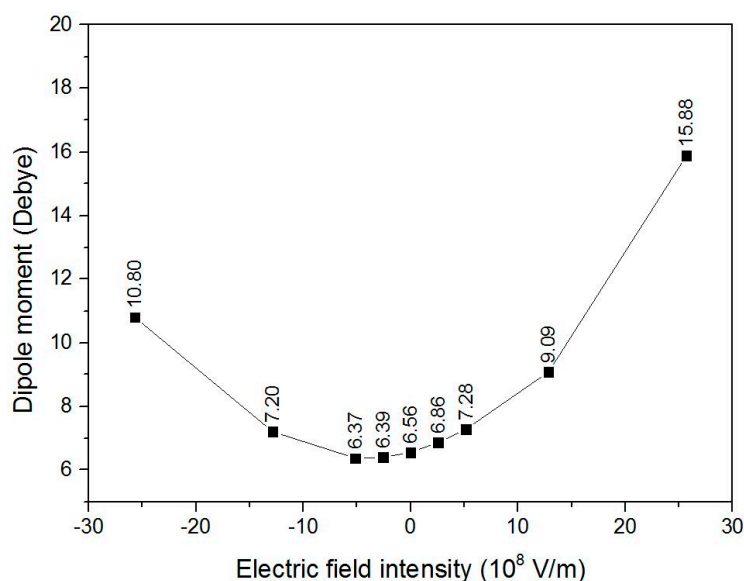


Figure 3. The dipole moment of the triolein molecule under different external electric field intensities.

The total energy of the triolein molecule was calculated and the results are shown in Figure 4. The total energy of the triolein molecule was found to first increase and then decrease as the external electric field intensity changed from -25.7×10^8 V/m to 25.7×10^8 V/m. The results are in accordance with those expected from Equations (1) and (2).

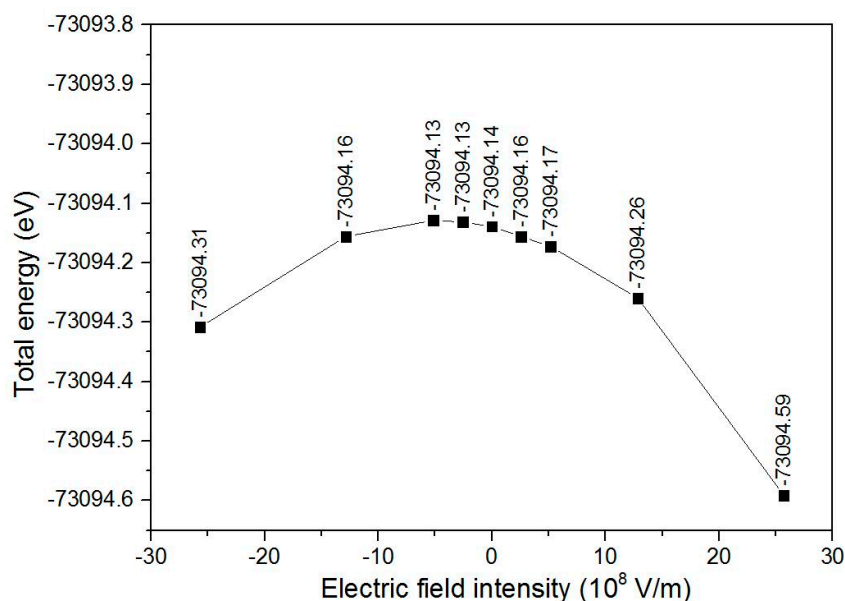


Figure 4. The total energy of the triolein molecule under different external electric field intensities.

3.3. Infrared Spectra of the Triolein Molecule under Different External Electric Fields

The IR spectra were calculated, and the results are shown in Figure 5. The spectra contain too much information to be completely analyzed. Some of the important vibrational frequencies of triolein are marked according to their corresponding wavenumbers in the spectra. Figure 5a shows the IR spectra

under no external electric field. The frequencies represented by wavenumbers 560.2 cm^{-1} , 560.4 cm^{-1} , and 560.6 cm^{-1} derive mainly from *cis* C=C rocking vibrations, including bonds C81=C83, C100=C102, and C119=C121. The frequency associated with 1123.4 cm^{-1} derives mainly from the C14-O10 stretching vibration. The frequencies associated with 1775.7 cm^{-1} , 1778.2 cm^{-1} , and 1784.9 cm^{-1} derive mainly from C=O stretching vibrations, including bonds C16=O17, C14=O15, and C12=O13. The vibrational frequencies associated with wavenumbers from 2887.1 cm^{-1} to 3018.5 cm^{-1} derive mainly from various types of C-H stretching vibrations.

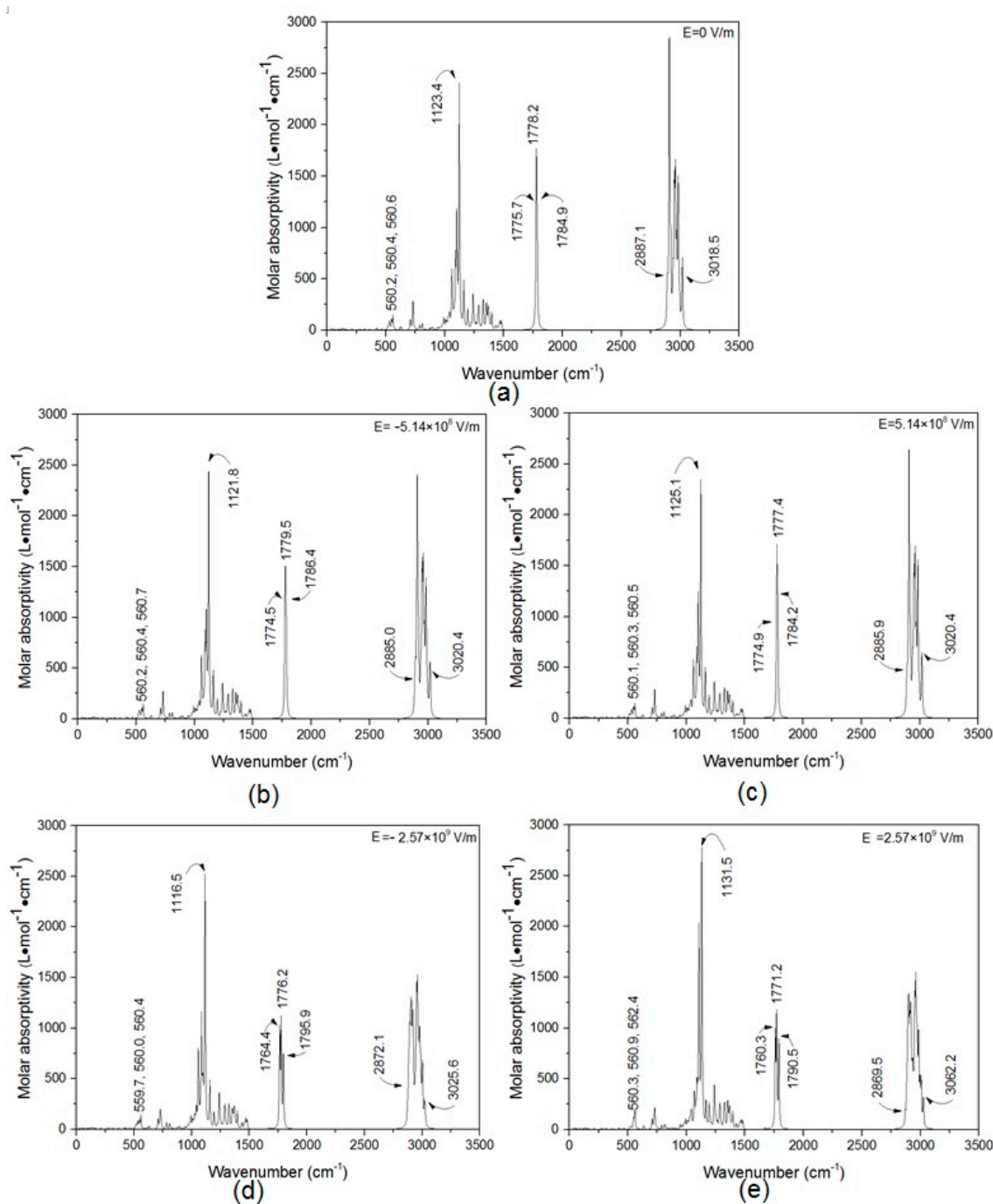


Figure 5. The infrared spectra of the triolein molecule under different external electric field intensities: 0 V/m (a); $-5.14 \times 10^8\text{ V/m}$ (b); $5.14 \times 10^8\text{ V/m}$ (c); $-2.57 \times 10^8\text{ V/m}$ (d); and $2.57 \times 10^8\text{ V/m}$ (e).

We note that a frequency shift, or the so called vibrational Stark effect, can be observed under the effect of an external electric field. The frequency of the C14-O10 stretching vibration is mainly associated with the 1123.4 cm^{-1} peak in Figure 5a under no external electric field; however, this stretching vibration shifts to 1116.5 cm^{-1} under an external electric field intensity of $-25.7 \times 10^8\text{ V/m}$ in Figure 5d, and to 1131.5 cm^{-1} under $25.7 \times 10^8\text{ V/m}$ in Figure 5e. The frequency of stretching vibrations, including bonds C16=O17, C14=O15, and C12=O13, is associated with wavenumbers $1775.7\text{--}1784.9\text{ cm}^{-1}$; however, this shifts to the range $1764.4\text{--}1759.9\text{ cm}^{-1}$ under an external electric field intensity of $-25.7 \times 10^8\text{ V/m}$, and to the range $1760.3\text{--}1790.5\text{ cm}^{-1}$ under $25.7 \times 10^8\text{ V/m}$. This is due to the fact that the frequency of the C=O stretching vibration undergoes a redshift or blueshift under an external electric field. The frequency band of C-H stretching vibrations is also extended, as shown in Figure 5. However, the frequencies of *cis* C=C rocking vibrations remain stable under external electric fields. Frequency shifts can be ascribed to changes in the bond lengths. For example, the frequency of the C14-O10 stretching vibration undergoes a blueshift of 8.1 cm^{-1} relative to the vibration frequency at no applied electric field because the bond length of *R*(C14-O10) shortens by 0.0112 \AA when an external electric field of $25.7 \times 10^8\text{ V/m}$ is applied.

3.4. Orbital Energies of the Triolein Molecule under Different External Electric Fields

An external electric field produces a drastic redistribution of orbitals, which depends on the response of the electron density. The highest occupied molecular orbital (HOMO) and the lowest unoccupied molecular orbital (LUMO) play an important role in the discharge property of a molecule. The HOMO and LUMO energies of the triolein molecule under different external electric fields are presented in Figure 6. We note that, with a variation in the external electric field intensity from $-25.7 \times 10^8\text{ V/m}$ to $25.7 \times 10^8\text{ V/m}$, the LUMO, LUMO+1, and LUMO+2 energies decrease continuously, while the HOMO, HOMO-1, and HOMO-2 energies decrease, and then increase.

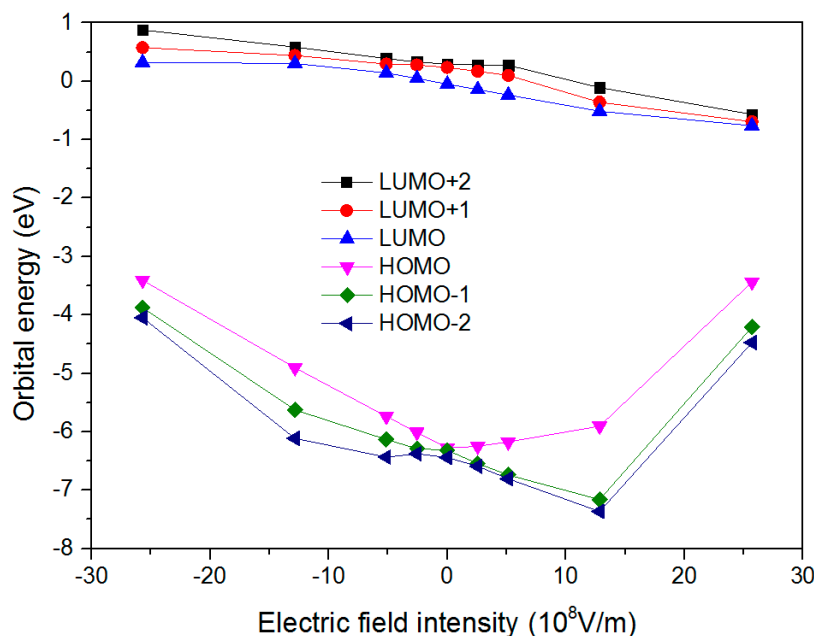


Figure 6. The highest occupied molecular orbital (HOMO) and the lowest unoccupied molecular orbital (LUMO) energies of the triolein molecule under different external electric field intensities.

The energy gap E_{HLG} between the HOMO and LUMO decreases with increasing external electric field intensity along both of the $\pm Z$ directions, as shown in Figure 7. The value of E_{HLG} often has a positive correlation with the chemical activity of free radicals. Hence, the triolein molecule is prone to being more lively with an increasing external electric field intensity.

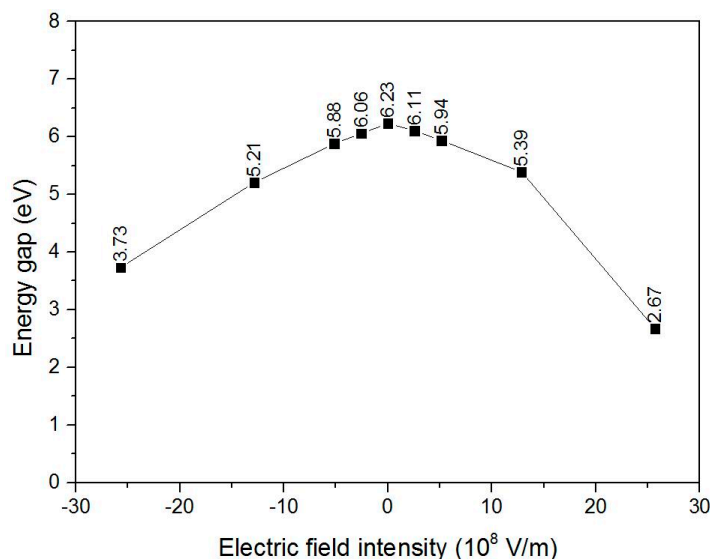


Figure 7. The energy gap E_{HLG} between the HOMO and LUMO of the triolein molecule under different external electric field intensities.

The evolution of the HOMO and LUMO of triolein under external electric fields is presented in Figure 8. When no external electric field is applied, the HOMO concentrates upon *cis* C100=C102. When an external electric field is applied, the electron cloud moves in an opposite direction to that of the electric field. In contrast, when no external electric field is applied, the LUMO concentrates upon *cis* C14=O15, and the electron cloud moves in the direction of the electric field when an external electric field is applied.

The composition of the HOMO and LUMO of the triolein molecule under different external electric fields was analyzed using a Mulliken partition by the Multiwfn program package [32]. The results are listed in Table 3. We note that, when no external electric field is applied, C100 and C102 make the primary contribution (39.67% and 39.66%, respectively) to the HOMO. In addition, C14 makes the primary contribution (52.51%) to the LUMO, while the neighbors of C14, i.e., O15 and O10, also make specific contributions (26.88% and 6.60%, respectively).

When an external electric field is applied, the HOMO moved smoothly to C81 and C83 (both contributions were about 40%), and was pushed to C85 (3.14%), C88 (4.33%), and C91 (1.72%) when an external electric field of 25.7×10^8 V/m was applied. As shown in Figure 6, the energy of the HOMO correspondingly increased. However, the LUMO remained at C14 and O15, and was centralized at C14 with increasing external electric field intensity. As shown in Figure 6, the energy of the LUMO correspondingly decreased slightly. With a negative external electric field intensity, the HOMO mainly concentrated at C100 and C102 (both contributions were about 40%), and was pushed to C107 (4.86%), C104 (3.49%), and C110 (2.62%) when an external electric field of -25.7×10^8 V/m was applied. Again, the energy of the HOMO increased. The LUMO moved to C16 and O17, and the energy of LUMO increased slightly with increasing external electric field intensity. This result is shown to be reasonable by the isosurfaces given in Figure 8.

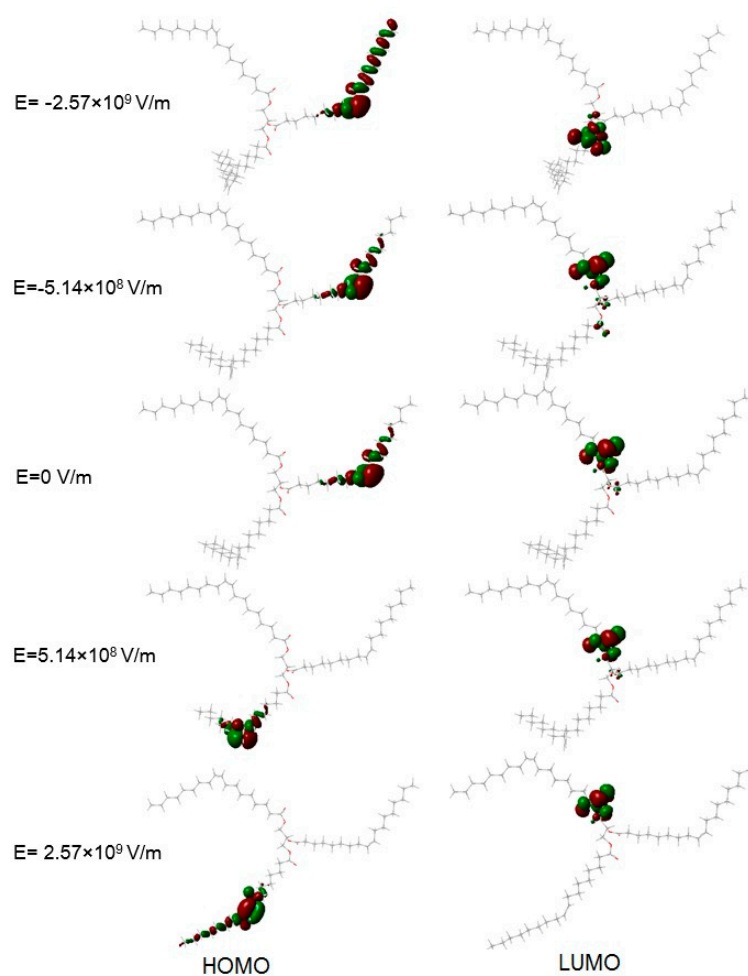


Figure 8. The evolution of the HOMO and LUMO of the triolein molecule under different external electric field intensities. Red: positive phase; green: Negative phase.

Table 3. Main compositions of the HOMO and LUMO of the triolein molecule (>1%) under different external electric field intensities.

E (10^8 V/m)		Main Composition of the HOMO and LUMO (%)
−25.7	HOMO	C100:37.00, C102:30.88, C107:4.86, C104:3.49, C110:2.62, C113:2.61, C116:2.55
	LUMO	C16:52.92, O17:26.39, O11:6.80, H21:5.86, H20:3.00, C18:2.23
−12.85	HOMO	C100:40.72, C102:37.70, C107:3.84, C63:3.06, C106:2.63, C104:2.74, H67:2.35
	LUMO	C16:51.03, O17:25.85, H21:5.29, H20:3.49, C18:2.17, C14:1.10
−5.14	HOMO	C100:40.20, C102:39.20, C107:3.59, C63:3.23, H106:2.53, H67:2.49, C104:2.43
	LUMO	C14:51.68, O15:26.64, O10:6.35, H30:4.83, H29:3.32, C27:2.20
−2.57	HOMO	C100:39.95, C102:39.35, C107:3.51, C63:3.32, C106:2.51, H67:2.50, C104:2.35
	LUMO	C14:52.29, O15:26.85, O10:6.49, H30:4.86, H29:3.36, C27:2.22
0	HOMO	C100:39.67, C102:39.65, C107:3.44, C63:3.40, H67:2.52, C106:2.50, C104:2.27
	LUMO	C14:52.51, O15:26.87, O10:6.58, H30:4.86, H29:3.38, C27:2.22
2.57	HOMO	C81:39.78, C83:39.77, C88:3.39, C51:3.36, H56:2.52, H86:2.52, C85:2.25
	LUMO	C14:52.65, O15:26.85, O10:6.66, H30:4.85, H29:3.39, C27:2.22
5.14	HOMO	C83:39.94, C81:39.80, C88:3.37, C51:3.36, H56:2.51, H86:2.49, C54:2.23
	LUMO	C14:52.75, O15:26.80, O10:6.74, H30:4.85, H29:3.40, C27:2.21
12.85	HOMO	C83:40.38, C81:39.89, C51:3.36, C88:3.32, H56:2.45, H86:2.44, C54:2.19
	LUMO	C14:53.01, O15:26.64, O10:6.96, H30:4.71, H29:3.50, C27:2.19
25.7	HOMO	C81:40.97, C83:35.21, C88:4.33, C85:3.14, H86:2.59, H56:2.26, C91:1.72
	LUMO	C14:53.32, O15:26.26, O10:7.53, H30:4.76, H29:3.51, C27:2.21

The HOMO and LUMO are considered to be related to the ionization potential (IP) and the electron affinity (EA), which are two main molecular descriptors that have been linked to the initiation and propagation of streamers in liquid dielectrics. The IP is a key parameter that determines the character of a streamer because streamer creation involves the loss of electrons from neutral oil molecules through ionization (e.g., field ionization, impact ionization, or photo-ionization). The IPs of triacylglycerol molecules strongly affect how fast and how far streamer propagation can progress. The EA has also been reported to be an important parameter for streamers originating from a negative electrode [33–38]. Koopman’s theorem states that the IP of a molecule is approximately equal to the product of -1 and the energy of the HOMO, while the EA is approximately equal to the product of -1 and the energy of the LUMO, which provides the estimated IP and EA values of triolein shown in Figure 9.

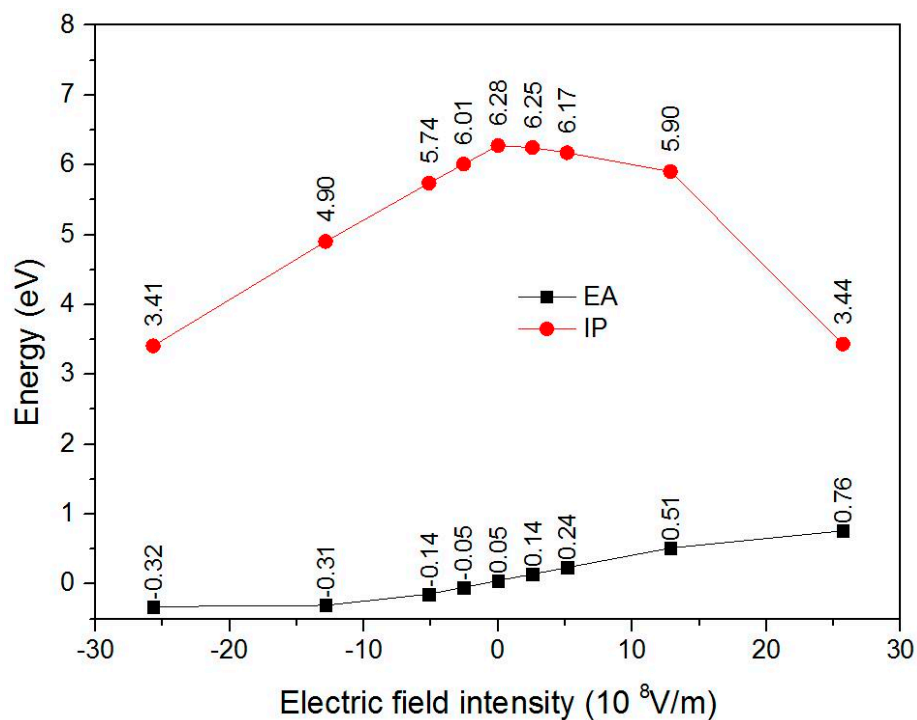


Figure 9. Estimated IP and EA values of the triolein molecule under different external electric field intensities.

From Figure 9, we see that the IP decreases with increasing external electric field intensity along both the $\pm Z$ directions. A decreasing IP facilitates the liberation of electrons from the triolein molecule and the propagation of a plasma channel in a high electric field. An approximate model for charge carrier production based on the Zener theory of tunneling in solids is usually applied to dielectric liquids to explain streamer propagation [39–41]. It is speculated that the rate of field ionization is proportional to the liquid’s density and inversely proportional to the IP of the molecule. The field ionization charge density rate is given as:

$$G(|E|) = \frac{e^2 n a |E|}{h} \exp\left[-\frac{\pi^2 m^* a (IP)^2}{eh^2 |E|}\right] \quad (4)$$

where $e = 1.6 \times 10^{-19}$ C is the electron charge, $h = 6.626 \times 10^{-34}$ $\text{m}^2 \cdot \text{kg} \cdot \text{s}^{-1}$ is Planck’s constant, $n \approx 10^{25} \text{ m}^{-3}$ is the number density of ionizable molecules, $a \approx 3.0 \times 10^{-10}$ m is the molecular separation, and $m^* \approx 9.11 \times 10^{-32}$ kg is the effective electron mass in the liquid. The value of G was estimated according to the above formula, and the results are shown in Figure 10. The value of G is 10^{17} – 10^{20} $\text{C} \cdot \text{m}^{-3} \cdot \text{s}^{-1}$ under an external electric field intensity of 2.57×10^8 – 25.7×10^8 V/m.

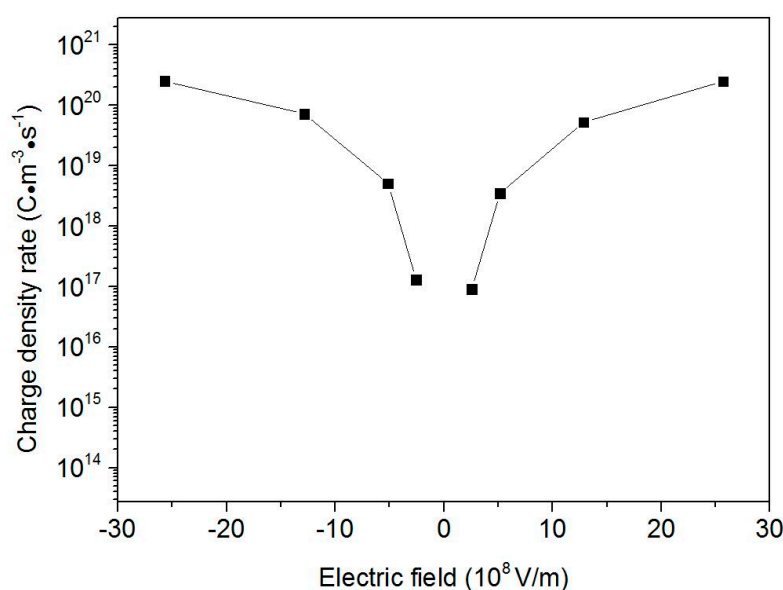


Figure 10. Field ionization charge density rate calculated from Equation (4) under different external electric field intensities.

Additionally, from Figure 9 we see that the EA increases from -0.32 eV to 0.76 eV when the external electric field varies from -25.7×10^8 V/m to 25.7×10^8 V/m. When $EA < 0$, the molecule tends toward charge neutrality. When $EA > 0$, the molecule tends to capture electrons. It can be speculated that some triacylglycerol molecules in the oil tend to remain neutral while others capture electrons to form negative ions. The formed negative ions neutralize the positive ions. Therefore, an increasing EA will restrain the production of charges under a high external electric field.

3.5. Excited States of the Triolein Molecule under Different External Electric Fields

The process of streamer initiation and propagation inevitably includes a luminous effect owing to the excited states of the molecules. As discussed in Section 2, TD-DFT calculations were conducted to estimate the influence of an external electric field on electronic excited states. The excitation energies E_{ex} , transition wavelengths λ , and oscillator strengths f of the first eight excited states are listed in Table 4. The values of E_{ex} of the first eight excited states tend to decrease with a decreasing external electric field along both the $\pm Z$ directions, and λ correspondingly increased because of the decreasing value of E_{HLG} . The values of f reflect the electron transition ability, which may be altered under an external electric field. For instance, with no external electric field, $f = 0$ for the seventh excited state, indicating that the electron transition is forbidden, whereas f is not zero when -25.7×10^8 V/m is applied.

Table 4. The excitation energies E_{ex} , transition wavelengths λ , and oscillator strengths f of the first eight excited states under different external electric field intensities.

E (10 ⁸ V/m)		$n = 1$	$n = 2$	$n = 3$	$n = 4$	$n = 5$	$n = 6$	$n = 7$	$n = 8$
-25.7	E_{ex} (eV)	5.68	5.71	5.72	5.92	5.96	6.05	6.11	6.12
	λ (nm)	218.33	217.28	216.94	209.43	208.05	205.10	202.88	202.68
	f	0.0005	0.0002	0.0006	0	0	0	0.0001	0
-12.85	E_{ex} (eV)	5.70	5.71	5.73	5.96	6.02	6.08	6.19	6.23
	λ (nm)	217.45	217.21	216.23	208.17	206.05	203.85	200.27	199.14
	f	0.0005	0.0006	0.0003	0	0	0	0	0

Table 4. Cont.

E (10^8 V/m)		$n = 1$	$n = 2$	$n = 3$	$n = 4$	$n = 5$	$n = 6$	$n = 7$	$n = 8$
−5.14	E_{ex} (eV)	5.70	5.71	5.74	5.98	6.05	6.10	6.23	6.29
	λ (nm)	217.44	217.2	216.14	207.44	204.8	203.11	199.16	197.48
	f	0.0005	0.0006	0.0003	0	0	0	0	0
−2.57	E_{ex} (eV)	5.70	5.71	5.74	5.98	6.06	6.11	6.23	6.29
	λ (nm)	217.54	217.17	216.16	207.23	204.46	202.89	198.9	197.12
	f	0.0005	0.0006	0.0004	0	0	0	0	0
0	E_{ex} (eV)	5.70	5.71	5.73	5.99	6.08	6.12	6.24	6.30
	λ (nm)	217.64	217.17	216.2	207.02	204.08	202.68	198.65	196.83
	f	0.0005	0.0006	0.0004	0	0	0	0	0
2.57	E_{ex} (eV)	5.69	5.71	5.73	6.00	6.09	6.12	6.25	6.30
	λ (nm)	217.75	217.2	216.25	206.79	203.69	202.45	198.41	196.68
	f	0.0005	0.0006	0.0004	0	0	0	0	0
5.14	E_{ex} (eV)	5.69	5.71	5.73	6.00	6.10	6.13	6.26	6.30
	λ (nm)	217.86	217.26	216.32	206.56	203.29	202.21	198.19	196.78
	f	0.0005	0.0007	0.0004	0	0	0	0	0
12.85	E_{ex} (eV)	5.68	5.70	5.73	6.03	6.14	6.16	6.26	6.27
	λ (nm)	218.16	217.56	216.54	205.78	202.01	201.39	198.06	197.71
	f	0.0005	0.0007	0.0004	0	0	0	0	0
25.7	E_{ex} (eV)	5.67	5.70	5.72	5.92	6.09	6.14	6.23	6.32
	λ (nm)	218.85	217.52	216.74	209.38	203.67	201.86	199.16	196.06
	f	0.0005	0.0006	0.0003	0	0	0	0	0

4. Conclusions

We investigated the influence of external electric fields at the magnitude for streamer initiation and propagation ranging from -25.7×10^8 V/m to 25.7×10^8 V/m along the Z axis on bond lengths, dipole moment, total energy, infrared spectra, and orbital energy of the triolein molecule by DFT with a B3LYP/6-31G* scheme. The excitation energies, transition wavelengths, and oscillator strengths of the first eight excited states under external electric fields were calculated using TD-DFT. The results provide the following conclusions.

- (1) The carbon-oxygen bond lengths change obviously with an increasing electric field intensity; however, the carbon-carbon bond lengths change slightly, although changes in the bond lengths are correlated with the direction of the electric field.
- (2) The resultant of the permanent dipole moment and the dipole moment induced by the external electric field decreased and then increased when an external electric field was applied along the $-Z$ direction, and increased continuously up to 15.88 Debye under an external electric field intensity of 25.7×10^8 V/m. Accordingly, the total energy increased and then decreased when the external electric field intensity varied from -25.7×10^8 V/m to 25.7×10^8 V/m.
- (3) Frequency shifts in IR spectra caused by external electric fields were observed. Frequency shifts were ascribed to changes in the bond lengths. The frequency bands of C-O stretching vibrations, C=O stretching vibrations, and C-H stretching vibrations were extended, while the frequencies of *cis* C=C rocking vibrations were stable under the external electric fields.
- (4) The electronic structure changed obviously under external electric fields. The energy of the HOMO increased with increasing external electric field intensity along both $\pm Z$ directions, which represented a corresponding decrease in the IP of the triolein molecule along the $\pm Z$ directions. The energy of the LUMO decreased continuously with the external electric field intensity varying from -25.7×10^8 V/m to 25.7×10^8 V/m, which represented a corresponding increase in the EA of the triolein molecule.

- (5) The excitation energies tended to decrease with a decreasing external electric field along both the $\pm Z$ directions because of the decreasing value of E_{HLG} .

Acknowledgments: The authors acknowledge National Science Foundation of China (No. 51425702) and the National Key Basic Research Program of China (973 program) (2015CB251003). We also appreciate the National “111” Project of the Ministry of Education of China (No. B08036) and the State Key Program of National Natural Science Foundation of China (U1537211). We acknowledge National Supercomputing Center in Shenzhen for providing the computational resources and Gaussian 09.

Author Contributions: All of the authors took part in this work as a team. Jian Li and Feipeng Wang designed the main theme of this paper. Yachao Wang and Jinghan Zhou developed the simulation model and completed the simulation. Suning Liang and Zhengyong Huang discussed the results and commented on the manuscript. All the authors read and reviewed the final manuscript.

Conflicts of Interest: The authors declare no conflict of interest.

References

- Oommen, T.V.; Claiborne, C.C.; Mullen, J.T. Biodegradable electrical insulation fluids. In Proceedings of the Electrical Insulation Conference and Electrical Manufacturing and Coil Winding Conference, Rosemont, IL, USA, 25–25 September 1997; pp. 465–468.
- Oommen, T.V. Vegetable oils for liquid-filled transformers. *IEEE Electr. Insul. Mag.* **2002**, *18*, 6–11. [[CrossRef](#)]
- McShane, C.P. Natural and synthetic ester dielectric fluids: Their relative environmental, fire safety, and electrical performance. In Proceedings of the IEEE Industrial and Commercial Power Systems Technical Conference, Sparks, NV, USA, 2–6 May 1999; pp. 8–9.
- Svoboda, M.; Trnka, P. Alternative electrical insulating fluids in power transformers. In Proceedings of the 15th International Scientific Conference on Electric Power Engineering, Brno, Czech Republic, 12–14 May 2014; pp. 399–402.
- Singh, J.; Sood, Y.R.; Jarial, R.K. Condition monitoring of power transformers—Bibliography survey. *IEEE Electr. Insul. Mag.* **2008**, *24*, 11–25. [[CrossRef](#)]
- Azis, N.; Jasni, J.; Kadir, M.; Mohtar, M.N. Suitability of palm based oil as dielectric insulating fluid in transformers. *J. Electr. Eng. Technol.* **2014**, *9*, 662–669. [[CrossRef](#)]
- Yang, L.J.; Liao, R.J.; Sun, C.X.; Zhu, M.Z. Influence of vegetable oil on the thermal aging of transformer paper and its mechanism. *IEEE Trans. Dielectr. Electr. Insul.* **2011**, *18*, 692–700. [[CrossRef](#)]
- Gockenbach, E.; Borsi, H. Natural and synthetic ester liquids as alternative to mineral oil for power transformers. In Proceedings of the Conference on Electrical Insulation and Dielectric Phenomena, Quebec, QC, Canada, 26–29 October 2008; pp. 521–524.
- Perrier, C.; Beroual, A. Experimental investigations on insulating liquids for power transformers: Mineral, ester and silicone oils. *IEEE Electr. Insul. Mag.* **2009**, *25*, 6–13. [[CrossRef](#)]
- Dang, V.H.; Beroual, A.; Perrier, C. Comparative study of streamer phenomena in mineral, synthetic and natural ester oils under lightning impulse voltage. In Proceedings of the International Conference on High Voltage Engineering and Application, New Orleans, LA, USA, 11–14 October 2010; pp. 560–563.
- Liu, Q.; Wang, Z.D. Streamer characteristic and breakdown in synthetic and natural ester transformer liquids under standard lightning impulse. *IEEE Trans. Dielectr. Electr. Insul.* **2011**, *18*, 285–294. [[CrossRef](#)]
- Dang, V.H.; Beroual, A.; Perrier, C. Investigations on streamers phenomena in mineral, synthetic and natural ester oils under lightning impulse voltage. *IEEE Trans. Dielectr. Electr. Insul.* **2012**, *19*, 1521–1527. [[CrossRef](#)]
- Liu, R.S.; Törnkvist, C. Ester fluids as alternative for mineral oil: The difference in streamer velocity and LI breakdown voltage. In Proceedings of the Annual Report Conference on Electrical Insulation and Dielectric Phenomena, Virginia Beach, VA, USA, 18–21 October 2009; pp. 543–548.
- Rapp, K.J.; Corkran, J.; McShane, C.P. Lightning impulse testing of natural ester fluid gaps and insulation interfaces. *IEEE Trans. Dielectr. Electr. Insul.* **2009**, *16*, 1595–1603. [[CrossRef](#)]
- Denat, A.; Lesaint, O. Breakdown of liquids in long gaps: Influence of distance, impulse shape, liquid nature, and interpretation of measurements. *IEEE Trans. Dielectr. Electr. Insul.* **2015**, *22*, 2581–2591. [[CrossRef](#)]
- Rapp, K.J.; McShane, C.P.; Vandermaar, J.; Vukovic, D.; Tenbohlen, S. Long gap breakdown of natural ester fluid. In Proceedings of the International Conference on High Voltage Engineering and Application, New Orleans, LA, USA, 11–14 October 2010; pp. 104–107.

17. Wedin, P. Electrical Breakdown in Dielectric Liquids—A Short Overview. *IEEE Electr. Insul. Mag.* **2014**, *30*, 20–25. [[CrossRef](#)]
18. Badent, R.; Hemmer, M.; Konekamp, U.; Julliard, Y.; Schwab, A.J. Streamer inception field strengths in rape-seed oils. In Proceedings of the Conference on Electrical Insulation and Dielectric Phenomena, Victoria, BC, Canada, 15–18 October 2000; pp. 272–275.
19. Tobazeon, R. Prebreakdown phenomena in dielectric liquids. *IEEE Trans. Dielectr. Electr. Insul.* **1994**, *1*, 1132–1147. [[CrossRef](#)]
20. Beroual, A.; Zahn, M.; Badent, A.; Kist, K.; Schwab, A.J.; Yamashita, H.; Yamazawa, K.; Danikas, M.; Chadband, W.D.; Torshin, Y. Propagation and structure of streamers in liquid dielectrics. *IEEE Electr. Insul. Mag.* **1998**, *14*, 6–17. [[CrossRef](#)]
21. Rozga, P. Streamer propagation in small gaps of synthetic ester and mineral oil under lightning impulse. *IEEE Trans. Dielectr. Electr. Insul.* **2015**, *22*, 1754–2762. [[CrossRef](#)]
22. Lída, M.; Holčápek, M. Triacylglycerols profiling in plant oils important in food industry, dietetics and cosmetics using high-performance liquid chromatography–atmospheric pressure chemical ionization mass spectrometry. *J. Chromatogr. A* **2008**, *1198–1199*, 115–130. [[CrossRef](#)] [[PubMed](#)]
23. Becke, A.D. Density-functional thermochemistry. III. The role of exact exchange. *J. Chem. Phys.* **1993**, *98*, 5648–5652. [[CrossRef](#)]
24. Lee, C.; Yang, W.; Parr, R.G. Development of the Colle-Salvetti correlation-energy formula into a functional of the electron density. *Phys. Rev. B* **1988**, *37*, 785–789. [[CrossRef](#)]
25. Buckingham, A.D. Direct method of measuring molecular quadrupole moments. *J. Chem. Phys.* **1959**, *30*, 1580–1585. [[CrossRef](#)]
26. Gisbergen, S.J.A.; Snijders, J.G.; Baerends, E.J. Implementation of time-dependent density functional response equations. *Comput. Phys. Commun.* **1999**, *118*, 119–138. [[CrossRef](#)]
27. Grozema, F.C.; Telesca, R.; Jonkman, H.T.; Siebbeles, L.D.A.; Snijders, J.G. Excited state polarizabilities of conjugated molecules calculated using time dependent density functional theory. *J. Chem. Phys.* **2001**, *15*, 10014–10021. [[CrossRef](#)]
28. Frisch, M.J.; Trucks, G.W.; Schlegel, H.B.; Scuseria, G.E.; Robb, M.A.; Cheeseman, J.R.; Scalmani, G.; Barone, V.; Mennucci, B.; Petersson, G.A.; et al. *Gaussian 09*; Gaussian Inc.: Wallingford, CT, USA, 2013.
29. The National Institute of Standards and Technology (NIST). Computational Chemistry Comparison and Benchmark Data Base. Available online: <http://cccbdb.nist.gov/vibscalejust.asp> (accessed on 31 October 2016).
30. Christy, A.A.; Xu, Z.F.; Harrington, P.D.B. Thermal degradation and isomerisation kinetics of triolein studied by infrared spectrometry and GC–MS combined with chemometrics. *Chem. Phys. Lipids* **2009**, *158*, 22–31. [[CrossRef](#)] [[PubMed](#)]
31. Kos, A.; Tefelski, D.B.; Kosciesza, R.; Rośtockci, A.J.; Roszkiewicz, A.; Ejchart, W.; Jastrzebski, C.; Siegoczyński, R.M. Certain physico-chemical properties of triolein and methyl alcohol–triolein mixture under pressure. *High Press. Res.* **2007**, *27*, 39–42. [[CrossRef](#)]
32. Lu, T.; Chen, F.W. *Multiscale 3.3.8*; Kein Research Center for Natural Sciences: Beijing, China, 2016.
33. Hebner, R.E.; Kelley, E.F.; Forster, E.O.; FitzPatrick, G.J. Observation of prebreakdown and breakdown phenomena in liquid hydrocarbons II: Non-uniform field conditions. *IEEE Trans. Electr. Insul.* **1985**, *20*, 281–292. [[CrossRef](#)]
34. Yamashita, H.; Forster, E.O.; Pompili, M. Streamer formation in perfluoropolyether under impulse conditions. *IEEE Trans. Electr. Insul.* **1993**, *28*, 324–329. [[CrossRef](#)]
35. Forster, E.O.; Yamashita, H.; Mazzetti, C.; Pompili, M.; Caroli, L.; Patrissi, S. The effect of the electrode gap on breakdown in liquid dielectrics. *IEEE Trans. Dielectr. Electr. Insul.* **1994**, *1*, 440–446. [[CrossRef](#)]
36. Nakao, Y.; Yamazaki, T.; Miyagi, K.; Sakai, Y.; Tagashira, H. The effect of molecular structure on prebreakdown phenomena in dielectric liquids under a nonuniform field. *Electr. Eng. Jpn.* **2002**, *139*, 1–8. [[CrossRef](#)]
37. Tsuchida, N. The electron affinity and ionization energy of various impurities in silicone oil. *IEEE Trans. Dielectr. Electr. Insul.* **1993**, *28*, 243–252. [[CrossRef](#)]
38. Smalø, H.S.; Åstrand, P.O. Calculation of ionization potentials and electron affinities for molecules relevant for streamer initiation and propagation. *IEEE Trans. Dielectr. Electr. Insul.* **2010**, *17*, 733–741. [[CrossRef](#)]
39. Zener, C. A theory of the electrical breakdown of solid dielectrics. *Proc. R. Soc. A* **1934**, *145*, 523–529. [[CrossRef](#)]

40. Sima, W.X.; Jiang, C.L.; Lewin, P.; Yang, Q.; Yuan, T. Modeling of the partial discharge process in a liquid dielectric: Effect of applied voltage, gap distance, and electrode type. *Energies* **2013**, *6*, 934–952. [[CrossRef](#)]
41. Jadidian, J.; Zahn, M.; Lavesson, N.; Widlund, O.; Borg, K. Effects of impulse voltage polarity, peak amplitude and rise time on streamer initiated from a needle electrode in transformer oil. *IEEE Trans. Plasma Sci.* **2012**, *40*, 909–918. [[CrossRef](#)]



© 2017 by the authors. Licensee MDPI, Basel, Switzerland. This article is an open access article distributed under the terms and conditions of the Creative Commons Attribution (CC BY) license (<http://creativecommons.org/licenses/by/4.0/>).